MOLECULAR IMAGING AND BIOLOGY

Mol Imaging Biol (2019) 21:567–573
DOI: 10.1007/s11307-018-1271-2

Published Online: 14 September 2018

RESEARCH ARTICLE

Inconsistent Detection of Sites of Metastatic Non-Clear Cell Renal Cell Carcinoma with PSMA-Targeted [^{18}F]DCFPyL PET/CT

Yafu Yin,[1,2] Scott P. Campbell,[3] Mark C. Markowski,[4] Philip M. Pierorazio,[3,4] Martin G. Pomper,[1,3,4] Mohamad E. Allaf,[3,4] Steven P. Rowe,[1,3] Michael A. Gorin[1,3,4]

[1]*The Russell H. Morgan Department of Radiology and Radiological Science, Johns Hopkins University School of Medicine, Baltimore, MD, USA*

[2]*Department of Nuclear Medicine, The First Hospital of China Medical University, Shenyang, China*

[3]*The James Buchanan Brady Urological Institute and Department of Urology, Johns Hopkins University School of Medicine, 600 North Wolfe Street, Park 213, Baltimore, MD, 21287, USA*

[4]*Department of Oncology, Sidney Kimmel Comprehensive Cancer Center, Johns Hopkins University School of Medicine, Baltimore, MD, USA*

Abstract

Purpose: To investigate the utility of prostate-specific membrane antigen (PSMA)-targeted [^{18}F]DCFPyL positron emission tomography (PET)/X-ray computed tomography (CT) imaging for the detection of sites of disease in patients with metastatic non-clear cell renal cell carcinoma (RCC).

Procedures: Eight patients with metastatic non-clear cell RCC underwent imaging with PSMA-targeted [^{18}F]DCFPyL PET/CT. Imaged RCC histologic subtypes included papillary RCC ($n = 3$), chromophobe RCC ($n = 2$), unclassified RCC ($n = 2$), and Xp11 translocation RCC ($n = 1$). Using comparison to conventional CT and/or magnetic resonance imaging as reference, two radiologists with expertise in nuclear medicine identified putative sites of disease on [^{18}F]DCFPyL PET/CT and classified each lesion as having no radiotracer uptake, equivocal uptake, or definitive uptake.

Resuts: In total, 73 metastatic sites and 3 primary tumors compatible with sites of non-clear cell RCC were identified on conventional imaging. Metastatic sites of disease included lymph nodes ($n = 40$), venous thrombi ($n = 3$), pulmonary nodules ($n = 10$), bone lesions ($n = 15$), brain lesions ($n = 3$), and retroperitoneal masses ($n = 2$). Only 10 of the 73 lesions (13.7 %) were classified as having definitive radiotracer uptake (median $SUV_{max} = 3.25$, range = 1.2–9.5), 14 lesions (19.2 %) had equivocal uptake (median $SUV_{max} = 2.85$, range = 0.5–6.5), and 49 lesions (67.1 %) had no definitive uptake above background (median $SUV_{max} = 1.7$, range = 0.2–3.0). The three primary renal tumors demonstrated lower radiotracer avidity relative to surrounding normal renal parenchyma.

Conclusions: A small proportion of sites of non-clear cell RCC showed uptake of the PSMA-targeted radiotracer [^{18}F]DCFPyL. Unlike for clear cell RCC, the results of this study indicate that PSMA-based PET is not appropriate for imaging other RCC subtypes.

Key words: Prostate-specific membrane antigen, Renal cell carcinoma, RCC, PSMA, [^{18}F]DCFPyL

Correspondence to: Michael Gorin; *e-mail:* mgorin1@jhmi.edu

Introduction

Renal cell carcinoma (RCC) is the most common primary malignancy of the kidney, with an annual global incidence of 425,000 cases per year [1]. At the time of initial diagnosis, 35 % of patients with RCC will present with metastatic disease, a condition that is near universally fatal. RCC is a general term used to describe a histologically and molecularly heterogeneous group of tumors that arise from the renal nephron. The most common subtypes of RCC are the clear cell (75 % of all RCCs), papillary (15 %), and chromophobe (5 %) histologies [2]. Less common histologic subtypes include collecting duct RCC, renal medullary carcinoma, mucinous tubular and spindle cell carcinoma, and MiT family translocation RCC [3].

At the present time, the detection of metastatic RCC is largely carried out with conventional cross-sectional imaging modalities including X-ray computed tomography (CT) and magnetic resonance imaging (MRI) [4, 5]. However, these anatomical imaging techniques are limited in their ability to characterize small sites of metastatic disease [6]. As an alternative, positron emission tomography (PET) utilizing the metabolic radiotracer 2-deoxy-2-[18F]fluoro-D-glucose (18F-FDG) has been studied for imaging metastatic RCC [7–9]. The sensitivity of this imaging test, however, is relatively low in comparison to conventional cross-sectional imaging and its role for monitoring response to treatment remains unclear.

To overcome the limitations of currently available imaging tests, a number of molecular imaging agents have been investigated for RCC [10, 11]. This includes small-molecule inhibitors of prostate-specific membrane antigen (PSMA), a type II transmembrane glycoprotein that is ubiquitously expressed on prostate cancer epithelial cells [12, 13] as well as endothelial cells within the neovasculature of a number of solid malignancies including RCC [14–22]. Owing to the abundant neovascularity and high degree of PSMA expression in clear cell RCC [23, 24], PSMA-targeted PET imaging has been of growing interest for the characterization of this malignancy, with some preliminary indications that PSMA-based PET may be more sensitive for sites of metastatic clear cell RCC than conventional imaging as well as [18F]FDG PET [21, 22, 25–31].

At the present time, the utility of PSMA-targeted PET imaging of non-clear cell RCCs is unknown. Although PSMA expression is commonly present in cases of non-clear cell RCC, it is found at lesser degree than for the clear cell subtype [32, 33]. Recently, three patients with metastatic non-clear cell RCC were reported in the literature to have been imaged with [68Ga]PSMA-11 PET/CT with variable success [25, 29]. Herein, we report the results of a small prospective study in which patients with metastatic non-clear cell RCC were imaged with PSMA-targeted [18F]DCFPyL PET/CT.

Materials and Methods

Patient Population

Eight patients with histologically proven non-clear cell RCC and conventional imaging findings compatible with metastatic disease were enrolled in a prospective study to broadly investigate the utility of [18F]DCFPyL PET/CT in patients with RCC (ClinicalTrials.gov Identifier NCT02687139). [18F]DCFPyL was synthesized as previously described [34], and the imaging protocol was performed in a manner consistent with the method described by Rowe and colleagues [21]. In brief, patients fasted from solid food for 4–6 h prior to intravenous injection of approximately 333 MBq (9 mCi) of the [18F]DCFPyL radiotracer. One hour following injection, a whole-body PET/CT was performed extending from the mid thighs to the vertex of the skull. In addition to imaging with [18F]DCFPyL PET/CT, all patients had previously undergone standard-of-care conventional cross-sectional imaging with CT or MRI of the chest, abdomen, and pelvis, with additional imaging of the brain as indicated by the presence of focal neurologic symptoms. Patients had typically been treated with multiple lines of systemic therapy at the time of [18F]DCFPyL imaging.

Image Analysis

All images were collaboratively reviewed by two nuclear medicine specialists with extensive experience in PET/CT imaging (YY and SPR). For each [18F]DCFPyL PET/CT, the following features were recorded: lesion location, lesion size, presence or absence of focal radiotracer uptake, and the maximum lean body mass-corrected standardized uptake value (SUV_{max}). The readers qualitatively categorized each lesion as having either no detectable radiotracer uptake, equivocal uptake, or definitive uptake. For primary renal lesions, tumor-to-background ratios (TBR) were calculated by dividing SUV_{max} of each lesion by SUV_{max} of the surrounding normal parenchyma.

Results

Between October 2015 and February 2017, eight patients were enrolled in this prospective study (median age 61, range 43–71 years). This included 3 (37.5 %) patients with papillary RCC, 2 (25.0 %) patients with chromophobe RCC, 2 (25.0 %) patients with unclassified RCC, and 1 (12.5 %) patient with Xp11 translocation RCC. [18F]DCFPyL PT/CT studies were performed a median of 21 days (range 2 to 44) following conventional imaging. Additional patient characteristics are provided in Table 1.

Table 1.. Patient characteristics and results of [18F]DCFPyL PET/CT imaging

Patient	Age (years)	Sex	Histologic subtype	Location of metastases	#Lesions	Definitive uptake	Equivocal uptake	No uptake	Median SUV_{max} (Range)
1	65	Male	Papillary RCC	Subdiaphragmatic mesenteric LNs	2		2		3.2(2.9– 3.5)
2	71	Female	Papillary RCC	Retroperitoneal mass	1		1		3.6(3.6)
3	63	Male	Papillary RCC	Retroperitoneal LNs	9		1	8	2.2(1.8– 4.1)
				Right renal vein thrombus	1		1		
4	58	Male	Unclassified RCC	Left parietal and temporal lobes	3	2	1		2.3(0.5– 6.2)
				Retroperitoneal Mass	1	1			
5	68	Male	Unclassified RCC	Bones	15		3	12	1.2(0.5–2.1)
6	43	Male	Chromophobe RCC	Left supraclavicular LNs	2		2		1.9(0.8– 2.8)
				Mesenteric LNs	3			3	
				Retroperitoneal LNs	12		1	11	
7	57	Male	Chromophobe RCC	Bilateral lower pulmonary lobes	10			10	1.4(0.2– 9.5)
				Retroperitoneal LNs	2		1	1	
				IVC thrombus	1	1			
				Left renal vein thrombus	1	1			
8	44	Female	Xp11 translocation RCC	Bilateral Supraclavicular LNs	5	5			2.7(1.7– 5.1)
				Retroperitoneal LNs	4		1	4	
				Retroperitoneal mass	1				
Total					73	10 (13.7 %)	14 (19.2 %)	49	(67.1 %)

Among the 8 patients, 73 putative sites of metastatic disease and 3 primary renal lesions (in two patients) were identified on the basis of conventional imaging. Metastatic sites of disease included lymph nodes ($n = 40$), venous thrombi ($n = 3$), pulmonary nodules ($n = 10$), bone lesions ($n = 15$), brain lesions (n = 3), and retroperitoneal masses ($n = 2$). In total, 10 of the 73 (13.7 %) suspected metastatic lesions were classified as having definitive radiotracer uptake on [18F]DCFPyL PET/CT imaging. An additional 14 (19.2 %) sites were classified as having equivocal uptake, and the remaining 49 (67.1 %) lesions were found to have no significant radiotracer uptake above background (Table 1). Overall, the median SUV_{max} of the 73 metastases was 1.9 (range 0.2–9.5), and the median diameter was 1.6 cm (range 0.6–9.0 cm) (Table 2). No lesions were identified on PET/CT without a corresponding finding on conventional imaging.

The ten lesions with definitive radiotracer uptake were identified in only 3 (37.5 %) of the 8 imaged patients. Radiotracer-avid lesions had a median diameter of 2.7 cm (range 1.1–6.2 cm) with a median SUV_{max} of 3.3 (range 1.2–9.5) (Table 2). One patient with unclassified RCC had three identifiable lesions on [18F]DCFPyL PET/CT, including two brain metastases ($SUV_{max} = 3.4$) and a retroperitoneal mass ($SUV_{max} = 6.2$) (Fig. 1). A third brain lesion in this patient was classified as having equivocal uptake ($SUV_{max} = 0.5$). A second patient with chromophobe RCC was found to have radiotracer uptake in thrombi of left renal vein ($SUV_{max} = 9.3$) and inferior vena cava ($SUV_{max} = 9.5$) (Fig. 2). This patient also had two retroperitoneal lymph nodes that lacked definitive radiotracer uptake and 10 pulmonary lesions with no uptake of radiotracer (Fig. 2). An additional five lesions with clearly definitive [18F]DCFPyL uptake (all supraclavicular lymph nodes) were identified in a third patient with Xp11 translocation RCC (median $SUV_{max} = 2.7$, range 1.7–5.1) (Fig. 3). This patient also had four sites of retroperitoneal lymphadenopathy and one retroperitoneal mass identified on CT. However, none of these lesions demonstrated significant radiotracer uptake (Fig. 3).

The 14 lesions with equivocal uptake had a median diameter of 3.2 cm (range 0.9–9.0 cm) with a median SUV_{max} of 2.9 (range 0.5–6.5), and the 49 lesions with no uptake had a median diameter of 1.5 cm (range 0.6–3.9 cm) with a median SUV_{max} of 1.7 (range

Table 2.. SUV_{max} and tumor diameter of definitive lesions, equivocal lesions, and lesions without radiotracer uptake

Radiotracer uptake (*n*)	Median SUV_{max} (range)	Median diameter (cm) (range)
Definitive (10)	3.25(1.2–9.5)	2.7 (1.1–6.2)
Equivocal (14)	2.85 (0.5–6.5)	3.2(0.9–9.0)
No uptake (49)	1.7 (0.2–3.0)	1.5 (0.6–3.9)
Total (73)	1.9 (0.2–9.5)	1.6 (0.6–9.0)

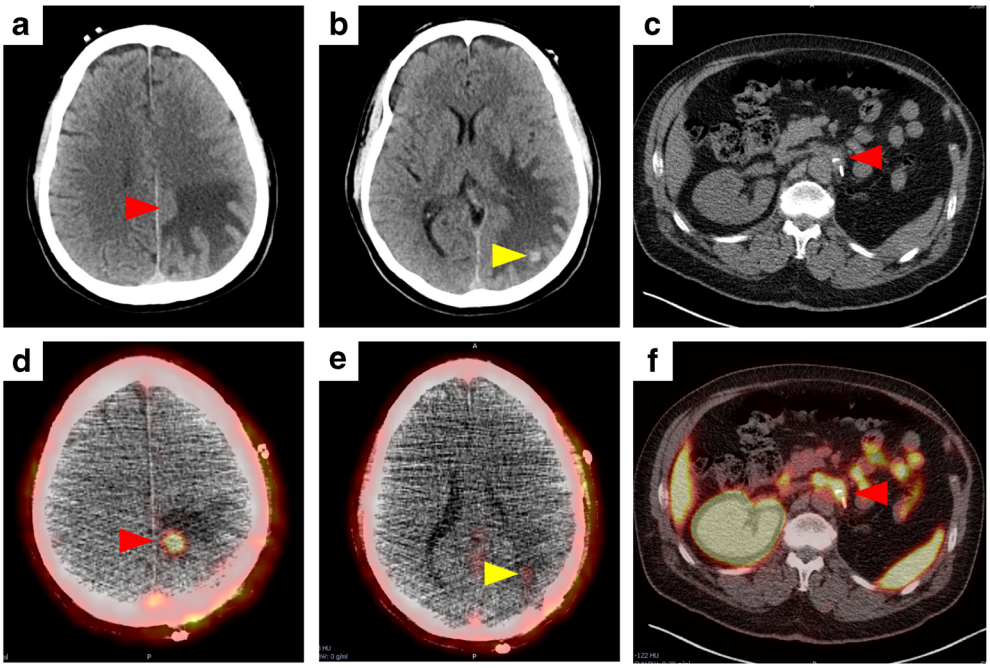

Fig. 1. Images of a patient with metastatic unclassified RCC. **a**, **b** Conventional imaging with CT demonstrated metastatic lesions within the brain as well as **c** a retroperitoneal mass. Imaging with [^{18}F]DCFPyL PET/CT demonstrated definitive uptake in **d** one of the brain lesions and **f** the retroperitoneal mass (red arrow) with SUV_{max} values of 3.4 and 6.2, respectively. **e** Equivocal radiotracer uptake was observed in the other intracranial lesion (yellow arrow, $SUV_{max} = 0.5$).

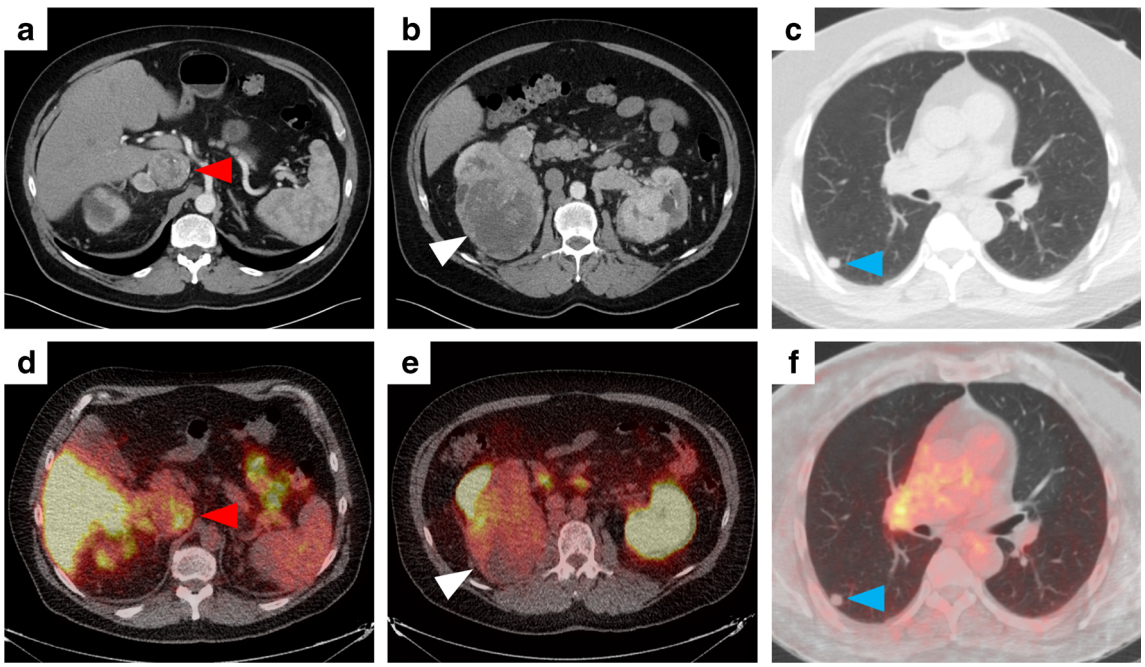

Fig. 2. Images of a patient with metastatic chromophobe RCC. CT imaging showed **a** an inferior vena cava thrombus, **b** a primary renal mass, and **c** multiple bilateral pulmonary nodules. **d** The inferior vena cava thrombus demonstrated avidity for [^{18}F]DCFPyL (red arrow, $SUV_{max} = 9.5$), whereas **e** the renal mass had heterogeneous uptake that was lower than the normal renal parenchyma (white arrow, $SUV_{max} = 9.3$, TBR = 0.1). **f** The pulmonary nodules had no detectable radiotracer uptake on [^{18}F]DCFPyL PET/CT (blue arrow, median $SUV_{max} = 1.1$, range 0.2–1.7).

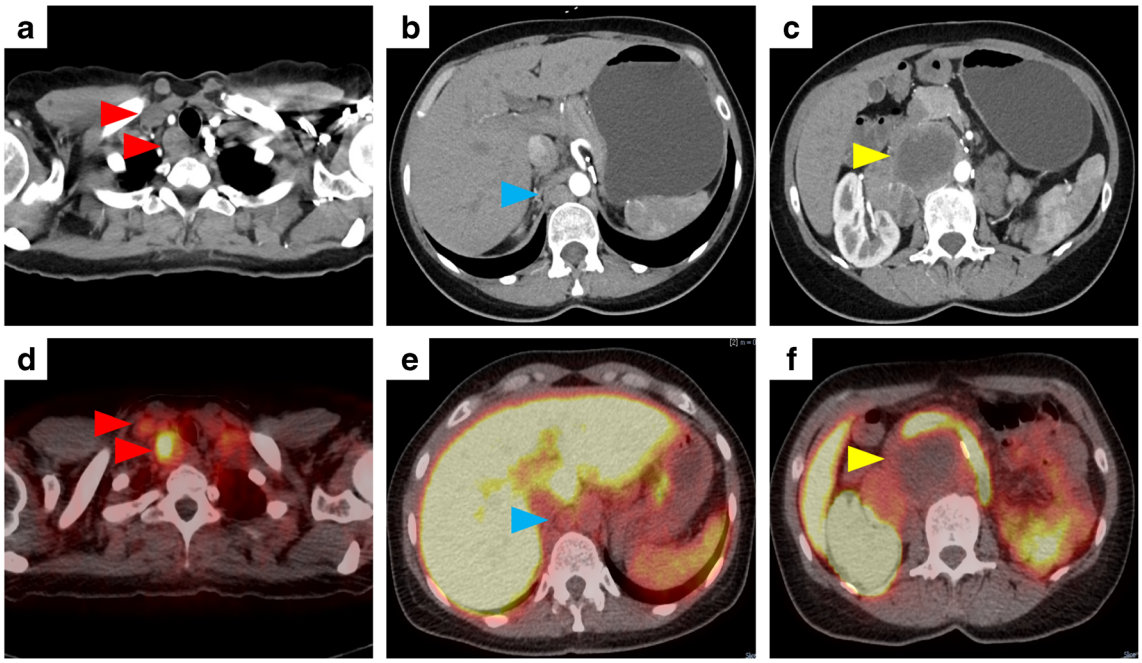

Fig. 3. Images of a patient with metastatic Xp11 translocation RCC. On CT, the patient was noted to have **a** metastatic supraclavicular lymph nodes, **b** enlarged retroperitoneal lymph nodes, and **c** a retroperitoneal mass. While the patient's **d** supraclavicular lymph nodes were identifiable on [18F]DCFPyL PET/CT (red arrows, median SUV_{max} = 2.7, range 1.7–5.1), **e** the retroperitoneal lymph nodes had no discernible radiotracer uptake (blue arrows, median SUV_{max} = 2.55, range 2.2–2.9). **f** The retroperitoneal mass had equivocal uptake (yellow arrow, SUV_{max} = 4.0).

0.2–3.0) (Table 2). Fifteen bone lesions were identified in one patient with unclassified RCC, and 10 pulmonary lesions were identified in one patient with chromophobe RCC; none of these lesions demonstrated definitive radiotracer uptake (Fig. 4).

The three primary renal lesions (one papillary RCC and two chromophobe RCCs) demonstrated lower uptake of radiotracer compared with the normal renal parenchyma (Figs. 2 and 5). SUV_{max} of the three primary lesions were 5.8 (TBR 0.3), 9.3 (TBR 0.1), and 11.6 (TBR 0.2).

Discussion

In this study, we observed inconsistent uptake of the PSMA-targeted PET radiotracer [18F]DCFPyL in eight patients with metastatic non-clear cell RCC. These results suggest that PSMA-targeted PET imaging of non-clear cell RCC is unlikely to play a significant role in this patient population and is inferior to conventional imaging with CT and/or MRI. Our findings are consistent with previously published reports in the pathology literature that showed present yet intermediate expression of PSMA in the neovasculature of non-clear cell RCC subtypes [32, 33].

Although our data suggest little utility of PSMA-targeted imaging for non-clear cell RCC, there is strong preliminary evidence to support a role for this class of radiotracers in patients with clear cell RCC [21, 22, 25–31]. In fact, currently available data suggest a higher sensitivity with PSMA-targeted PET for detecting sites of metastatic disease

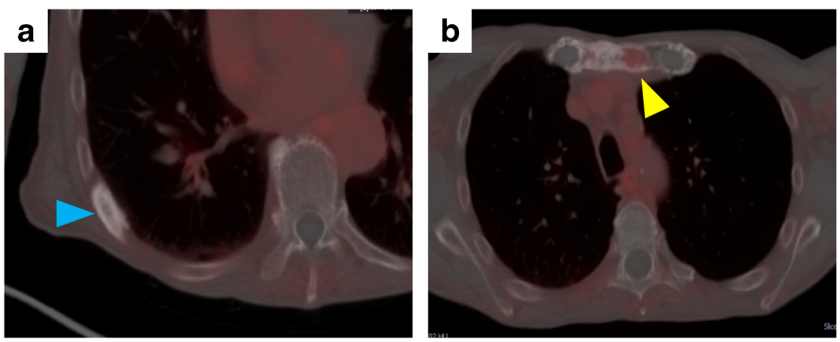

Fig. 4. [18F]DCFPyL PET/CT images of a patient with metastatic unclassified RCC. Multiple bone metastases were observed that had **a** no (blue arrow, SUV_{max} = 0.5) or **b** equivocal (yellow arrow SUV_{max} = 2.1) uptake of the [18F]DCFPyL radiotracer.

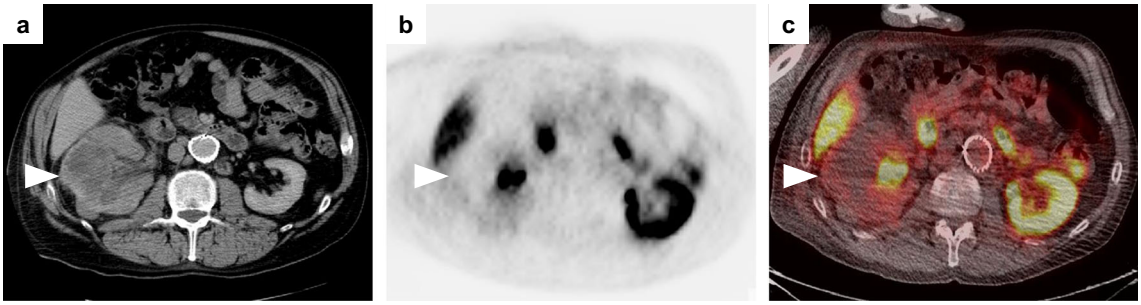

Fig. 5. Images of primary renal lesion in a patient with papillary RCC. **a** The large left renal tumor can be readily seen on CT (white arrow). **b** The PET and **c** fused PET/CT images demonstrated radiotracer uptake that was markedly lower than that of the normal left renal parenchyma (white arrows, $SUV_{max} = 5.8$, TBR = 0.3).

than with conventional imaging. However, these data require confirmation in large prospective trials and the therapeutic implications of this improvement in sensitivity remain unclear. Furthermore, there may be role for endoradiotherapy in patients with clear cell RCC with PSMA-targeted agents conjugated to α- or β-emitting therapeutic radionuclides [35]. It is worth noting that although PSMA-targeted PET appears to have a limited role in imaging all-comers with non-clear cell RCC, it is conceivable that endoradiotherapy directed against PSMA can be used in select patients with metastatic non-clear cell RCC that have exhausted all potential lines of conventional therapy and show uptake with PSMA-targeted imaging. However, based on our data, we acknowledge that this circumstance is likely to be quite uncommon.

The present study is not without limitations. Most notably, this study was comprised of a small number of patients with multiple non-clear cell RCC histologic subtypes, thus limiting the definitiveness of our observations. Additionally, patients in this study had received a number of different therapies prior to being imaged; therefore, it is unknown whether some of the lesions that lacked radiotracer uptake or had equivocal levels of uptake might reflect some degree of treatment effect. Nonetheless, the difference in lesion detection efficiency between conventional imaging and [18F]DCFPyL was pronounced and unlikely to have been fully explained by prior treatment.

Conclusions

Although PSMA-targeted radiotracers such as [18F]DCFPyL have been previously shown to have high detection rates for lesions in patients with metastatic clear cell RCC, the low and inconsistent uptake of these agents in cases of non-clear cell RCC suggest that PSMA-targeted PET is not appropriate for imaging this patient population.

Sources of Funding

Charitable gifts to The James Buchanan Brady Urological Institute.

Compliance with Ethical Standards

Conflict of Interest

MGP is a co-inventor on a United States Patent covering [18F]DCFPyL and as such is entitled to a portion of any licensing fees and royalties generated by this technology. MAG has served as a consultant to Progenics Pharmaceuticals, the licensee of [18F]DCFPyL. MAG and SPR have received research support from Progenics Pharmaceuticals.

References

1. Fitzmaurice C, Allen C, Barber RM et al (2017) Global, regional, and National Cancer Incidence, mortality, years of life lost, years lived with disability, and disability-adjusted life-years for 32 cancer groups, 1990 to 2015: a systematic analysis for the global burden of disease study. JAMA Oncol 3:524–548
2. Frank I, Blute ML, Cheville JC et al (2003) Solid renal tumors: an analysis of pathological features related to tumor size. J Urol 170:2217–2220
3. Tickoo SK, Gopalan A (2008) Pathologic features of renal cortical tumors. Urol Clin North Am 35:551–561
4. Campbell S, Uzzo RG, Allaf ME, Bass EB, Cadeddu JA, Chang A, Clark PE, Davis BJ, Derweesh IH, Giambarresi L, Gervais DA, Hu SL, Lane BR, Leibovich BC, Pierorazio PM (2017) Renal mass and localized renal cancer: AUA guideline. J Urol 198:520–529
5. Ljungberg B, Bensalah K, Canfield S, Dabestani S, Hofmann F, Hora M, Kuczyk MA, Lam T, Marconi L, Merseburger AS, Mulders P, Powles T, Staehler M, Volpe A, Bex A (2015) EAU guidelines on renal cell carcinoma: 2014 update. Eur Urol 67:913–924
6. Brufau BP, Cerqueda CS, Villalba LB, Izquierdo RS, González BM, Molina CN (2013) Metastatic renal cell carcinoma: radiologic findings and assessment of response to targeted antiangiogenic therapy by using multidetector CT. Radiographics 33:1691–1716
7. Wang HY, Ding HJ, Chen JH, Chao CH, Lu YY, Lin WY, Kao CH (2012) Meta-analysis of the diagnostic performance of [18F]FDG-PET and PET/CT in renal cell carcinoma. Cancer Imaging 12:464–474
8. Liu Y (2016) The place of FDG PET/CT in renal cell carcinoma: value and limitations. Front Oncol 6:201
9. Caldarella C, Muoio B, Isgro MA et al (2014) The role of fluorine-18-fluorodeoxyglucose positron emission tomography in evaluating the response to tyrosine-kinase inhibitors in patients with metastatic primary renal cell carcinoma. Radiol Oncol 48:219–227
10. Gorin MA, Rowe SP, Allaf ME (2015) Nuclear imaging of renal tumours: a step towards improved risk stratification. Nat Rev Urol 12:445–450
11. Khandani AH, Rathmell WK (2012) Positron emission tomography in renal cell carcinoma: an imaging biomarker in development. Semin Nucl Med 42:221–230
12. Silver DA, Pellicer I, Fair WR, Heston WD, Cordon-Cardo C (1997) Prostate-specific membrane antigen expression in normal and malignant human tissues. Clin Cancer Res 3:81–85

13. Bander NH (2006) Technology insight: monoclonal antibody imaging of prostate cancer. Nat Clin Pract Urol 3:216–225
14. Salas Fragomeni RA, Amir T, Sheikhbahaei S, Harvey SC, Javadi MS, Solnes LB, Kiess AP, Allaf ME, Pomper MG, Gorin MA, Rowe SP (2018) Imaging of non-prostate cancers using PSMA-targeted radiotracers: rationale, current state of the field, and a call to arms. J Nucl Med 59:871–877
15. Verburg FA, Krohn T, Heinzel A, Mottaghy FM, Behrendt FF (2015) First evidence of PSMA expression in differentiated thyroid cancer using [68Ga]PSMA-HBED-CC PET/CT. Eur J Nucl Med Mol Imaging 42:1622–1623
16. Sasikumar A, Joy A, Nanabala R, Pillai MRA, Thomas B, Vikraman KR (2016) 68Ga-PSMA PET/CT imaging in primary hepatocellular carcinoma. Eur J Nucl Med Mol Imaging 43:795–796
17. Sasikumar A, Joy A, Pillai MR et al (2017) Diagnostic value of 68Ga PSMA-11 PET/CT imaging of brain tumors-preliminary analysis. Clin Nucl Med 42:e41–e48
18. Sasikumar A, Joy A, Pillai MRA, Alex TM, Narayanan G (2017) 68Ga-PSMA PET/CT in osteosarcoma in fibrous dysplasia. Clin Nucl Med 42:446–447
19. Sasikumar A, Joy A, Pillai M, S B, SR S (2017) 68Ga-PSMA uptake in an incidentally detected gastrointestinal stromal tumor in a case of suspected carcinoma prostate. Clin Nucl Med 42:e447–e448
20. Sathekge M, Lengana T, Modiselle M, Vorster M, Zeevaart JR, Maes A, Ebenhan T, van de Wiele C (2017) 68Ga-PSMA-HBED-CC PET imaging in breast carcinoma patients. Eur J Nucl Med Mol Imaging 44:689–694
21. Rowe SP, Gorin MA, Hammers HJ, Som Javadi M, Hawasli H, Szabo Z, Cho SY, Pomper MG, Allaf ME (2015) Imaging of metastatic clear cell renal cell carcinoma with PSMA-targeted 18F-DCFPyL PET/CT. Ann Nucl Med 29:877–882
22. Rowe SP, Gorin MA, Hammers HJ, Pomper MG, Allaf ME, Javadi MS (2016) Detection of 18F-FDG PET/CT occult lesions with 18F-DCFPyL PET/CT in a patient with metastatic renal cell carcinoma. Clin Nucl Med 41:83–85
23. Chang SS, Reuter VE, Heston WD, Gaudin PB (2001) Metastatic renal cell carcinoma neovasculature expresses prostate-specific membrane antigen. Urology 57:801–805
24. Campbell SP, Baras AS, Ball MW, Kates M, Hahn NM, Bivalacqua TJ, Johnson MH, Pomper MG, Allaf ME, Rowe SP, Gorin MA (2018) Low levels of PSMA expression limit the utility of 18F-DCFPyL PET/CT for imaging urothelial carcinoma. Ann Nucl Med 32:69–74
25. Rhee H, Blazak J, Tham CM, Ng KL, Shepherd B, Lawson M, Preston J, Vela I, Thomas P, Wood S (2016) Pilot study: use of gallium-68 PSMA PET for detection of metastatic lesions in patients with renal tumour. EJNMMI Res 6:76
26. Sasikumar A, Joy A, Nanabala R, Unni M, TK P (2016) Complimentary pattern of uptake in 18F-FDG PET/CT and 68Ga-prostate-specific membrane antigen PET/CT in a case of metastatic clear cell renal carcinoma. Clin Nucl Med 41:e517–e519
27. Rhee H, Ng KL, Tse BW et al (2016) Using prostate specific membrane antigen (PSMA) expression in clear cell renal cell carcinoma for imaging advanced disease. Pathology 48:613–616
28. Gorin MA, Rowe SP, Hooper JE, Kates M, Hammers HJ, Szabo Z, Pomper MG, Allaf ME (2017) PSMA-targeted 18F-DCFPyL PET/CT imaging of clear cell renal cell carcinoma: results from a rapid autopsy. Eur Urol 71:145–146
29. Siva S, Callahan J, Pryor D, Martin J, Lawrentschuk N, Hofman MS (2017) Utility of 68Ga prostate specific membrane antigen - positron emission tomography in diagnosis and response assessment of recurrent renal cell carcinoma. J Med Imaging Radiat Oncol 61:372–378
30. Demirci E, Ocak M, Kabasakal L, Decristoforo C, Talat Z, Halaç M, Kanmaz B (2014) 68Ga-PSMA PET/CT imaging of metastatic clear cell renal cell carcinoma. Eur J Nucl Med Mol Imaging 41:1461–1462
31. Sawicki LM, Buchbender C, Boos J, Giessing M, Ermert J, Antke C, Antoch G, Hautzel H (2017) Diagnostic potential of PET/CT using a 68Ga-labelled prostate-specific membrane antigen ligand in whole-body staging of renal cell carcinoma: initial experience. Eur J Nucl Med Mol Imaging 44:102–107
32. Baccala A, Sercia L, Li J, Heston W, Zhou M (2007) Expression of prostate-specific membrane antigen in tumor-associated neovasculature of renal neoplasms. Urology 70:385–390
33. Spatz S, Tolkach Y, Jung K, Stephan C, Busch J, Ralla B, Rabien A, Feldmann G, Brossart P, Bundschuh RA, Ahmadzadehfar H, Essler M, Toma M, Müller SC, Ellinger J, Hauser S, Kristiansen G (2018) Comprehensive evaluation of prostate specific membrane antigen expression in the vasculature of renal tumors: implications for imaging studies and prognostic role. J Urol 199:370–377
34. Ravert HT, Holt DP, Chen Y, Mease RC, Fan H, Pomper MG, Dannals RF (2016) An improved synthesis of the radiolabeled prostate-specific membrane antigen inhibitor, [18F]DCFPyL. J Labelled Comp Radiopharm 59:439–450
35. Gorin MA, Rowe SP (2017) Kidney cancer: PSMA: a potential therapeutic target in RCC. Nat Rev Urol 14:646–647